Sensitivity of WFIRST Coronagraph Broadband Contrast Performance to DM Actuator Errors

Erkin Sidick*, Byoung-Joon Seo, Brian Kern, Ilya Poberezhskiy, Bijan Nemati, and John T. Trauger
Jet Propulsion Laboratory, California Institute of Technology, 4800 Oak Grove Drive, Pasadena, CA 91109

ABSTRACT

The WFIRST/AFTA 2.4 m space telescope currently under study includes a stellar coronagraph for the imaging and the spectral characterization of extrasolar planets. The coronagraph employs sequential deformable mirrors to compensate for phase and amplitude errors. Using the optical model of an Occulting Mask Coronagraph (OMC) testbed at the Jet Propulsion Laboratory (JPL), we have investigated the sensitivity of a Hybrid Lyot Coronagraph (HLC) broadband contrast performance to DM actuator errors and actuator limits. Considered case include drifts in actuator gains or actuator response curves, paired actuators, as well as the limits imposed by a neighboring-actuator rule. Actual data about the actuator drifts and the knowledge about the paired-actuators obtained in several DM characterization experiments conducted at JPL, as well as the neighboring-actuator rule implemented on the OMC testbed were used in simulations. We obtained good agreement between the model prediction and the testbed measurement in terms of static HLC contrast floor and contrast chromaticity.

Keywords: Coronagraphy, adaptive optics, deformable mirrors, space telescopes, exoplanets

1. INTRODUCTION

The WFIRST-AFTA coronagraph is baselined to use two separate but compatible modes, a Hybrid Lyot Coronagraph (HLC) [1-4] and a Shaped-Pupil Coronagraph [5-6]. Another design is based around a Phase-Induced Amplitude Apodization Complex-Mask Coronagraph (PIAACMC) [7-8], and is being matured as a backup. A catch-all term, Occulting Mask Coronagraph or OMC, is being used for the combination of the HLC and the SPC in a single instrument [6]. Recently, the OMC project team at JPL has successfully completed Milestone 9. Among the two OMC configurations, the static HLC testbed achieved a mean contrast of $1.6\text{x}10^{-9}$ (modulated plus unmodulated components) with 10% broadband light centered at 550 nm in a full 360-deg dark-hole with a working angle between $3\lambda/D$ and $9\lambda/D$ with arbitrary polarization. The OMC relies on a wavefront control (WFC) algorithm called Electric-Field Conjugation (EFC) to obtain such high contrast [9]. On the OMC testbed, this algorithm works with two 48x48 actuators deformable mirrors (DM's) to create a "dark-hole" in a predefined region of the image plane where terrestrial planets would be found. It achieves the desired high contrast level in two stages. The first is the estimation stage. In this stage, the algorithm provides an estimate of the aberrated complex electric-field (e-field) in the image plane based on pairs of images taken at the final image plane using different DM command patterns [10]. The second is the WFC or the EFC stage. In this stage the algorithm generates a correction based on the estimated e-field of the first stage. The correction is then applied to the DM actuators to null the image plane e-field in the predefined dark-hole region. This process is carried out iteratively, with both stages repeated in each iteration.

We have investigated the effects of the DM actuator constraints and errors on the efficiency of the EFC algorithm, achievable contrast floor as well as contrast chromaticity. Considered cases include actuator command limit, neighboring actuator rule, paired actuators, and random actuator gain errors associated with two DM's being used on the current OMC testbed. The structural design of the optical model as well as the parameters of various optical elements used in the analysis are drawn from the current HLC testbed system that have been implemented with two DM's. The optical model uses a pair of pupil-plane amplitude and phase directly measured on the HLC testbed, and the alignment parameters of the DM1, DM2, Occulting-Mask and Lyot-Stop that have also been obtained from the testbed by best effort. The optical simulation algorithm uses compact PROPER simulation software [11]. This paper presents results on the effects of DM actuator constraints and actuator gain errors on the control of the e-field at the final image-plane of

*Erkin.Sidick@jpl.nasa.gov; Phone 1 818 393-7585; Fax 1 818 393-3290; www.jpl.nasa.gov

HLC when the light source is a 10%-bandwidth broad-band beam. It will be shown that the predicted contrast behavior of the HLC agrees well with what was observed on the testbed. A new actuator regularization scheme, or "β-schedule", is used in the simulations of this paper as well as on the OMC testbed. It works better than the conventional approach that we have reported in the past. The reason why the new β-schedule works better was explained in detail in our companion paper [12]. That reference also contains some important background information about our model and the HLC testbed that is not included in this paper.

The DMs currently being used on the OMC testbed at JPL are manufactured by Northrop Grumman Xinetics, and are similar to the ones that have been in continuous use in HCIT testbed for over 10 years. They are described in detail in Ref. [4]. Some of the previous studies conducted about the effects of Xinetics DM actuator errors on coronagraph contrast performance can be found in Refs. [13-16]. Among them, Ref. [13] studies the effects of random actuator gain errors, asymmetric actuator gain errors, the nonlinearity in DM actuator response to the applied control voltages, and bad (or dead) actuators on the efficiency of the broadband EFC algorithm. Ref. [14] experimentally confirms the predicted broadband contrast behavior of the HCIT when 1 – 4 pairs of actuators in a DM are pegged (frozen). Ref. [15] investigates the effects of actuator gain calibration errors and actuator command digitization errors on the performance of HLC's Low-Order Wavefront Sensing and Control (LOWFS/C) subsystem. And Ref. [16] examines how the lateral and the longitudinal translation errors and clocking errors of DM1 and DM2, as well as the mismatch errors in actuator response between the testbed and model affect the broadband contrast performance of the HLC. Because the important background information about our model and the HLC testbed has already been presented in our companion paper [12], we directly go into the discussion of the main subjects in this paper.

2. EFFECTS OF ACTUATOR CONSTRAINTS ON CONTRAST

On the OMC testbed, the actuator commands are applied in units of voltage (V) about a bias level, such as 30V or 50V. In simulations we use actuator heights in nanometer (nm) directly, usually in the range of -250nm to 250nm. This corresponds to a peak-to-valley (PV) pupil phase change of ±500nm (when converted to an Optical Path Difference, OPD, at 550nm wavelength). The actuator commands in V and the actuator heights (or strokes) in nm are related by an actuator gain map having a unit of nm/V. The actuator constraint of the DMs currently being used on the OMC testbed have the following three main components:

(1) Actuator commands must be in the 0 – 100V range,
(2) The absolute value of the difference of any two adjacent (or neighboring) actuators cannot be more than 30V (this is called "neighboring-rule"), or $|\Delta V| \leq 30V$,
(3) Two pairs of actuators in DM1 are interconnected (or paired).

The third component above is actually a defect of DM1, but we chose to include it in the actuator constraint for convenience. On the DM coordinate system of the HLC model, the actuator at Row = 1 and Column = 1, or Act(1,1), is located at the lowest left corner, and the two pairs of interconnected actuators are Act(29-30,41) and Act(12-13,12), respectively.

There are two components in DM actuator commands. The first is the "phase-flattening component" and it is used to flatten the system pupil wavefront phase errors. The second is the "dark-hole component" and it is used to generate a dark-hole. Figures 1(a,b) are one examples of DM1 and DM2 actuator commands used to flatten the phase errors of the HLC system. Figures 1(c,d) show the examples of DM1 and DM2 actuator gains measured on the HLC testbed.

When we carry out broadband EFC simulations, we implement the actuator constraint in the following way: First, we convert the actuator heights from nm into volts using the actuator gain map in Figs. 1(c,d). Then add these actuator commands to the ones in Figs. 1(a,b). After that truncate the out-of-range actuator commands either to 0V or 100V, fix the neighboring-rule violations, and change the command of each paired actuators to their average value. We repeat this process for every EFC iteration.

Actuator constraint degrades the efficiency of an EFC process in two main ways. The first, it reduces the convergence speed. That is, with actuator constraint, it requires a larger number of EFC iterations to achieve the same level of contrast floor. The second, it raises the final achievable contrast floor. The results shown in Figs. 2(a,b) reveal such a fact. Figure 2(a) shows the 10% broadband mean contrast, C_{bb}, as a function of control or EFC iterations, and Fig. 2(b) plots the corresponding actuator regularization coefficient, or the β-values used [12]. In Fig. 2(a), the red-curve was obtained without including the actuator constraint, and the blue-one with the actuator constraint included. The figure

legends list the final C_{bb} – values obtained in these simulations. As is seen from part (a), the actuator constraint degrades the mean contrast by more than 2x in this particular case.

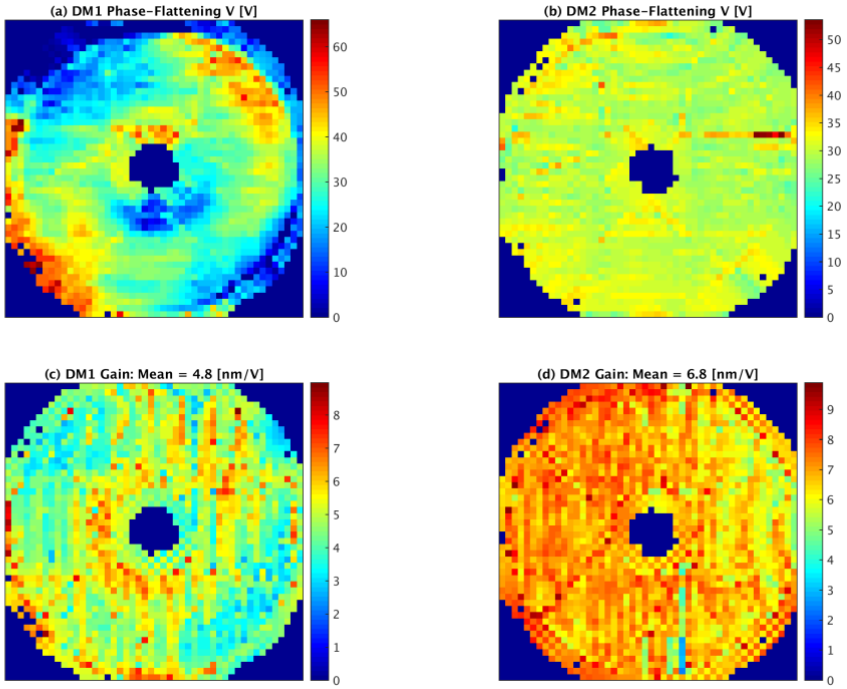

Figure 1. (a,b) Examples of the phase-flattening components of the DM1 and DM2 commands measured on the HLC testbed. (c,d) Examples of DM actuator gains measured on the HLC testbed. Only the data of the "active" actuators used in simulations are shown.

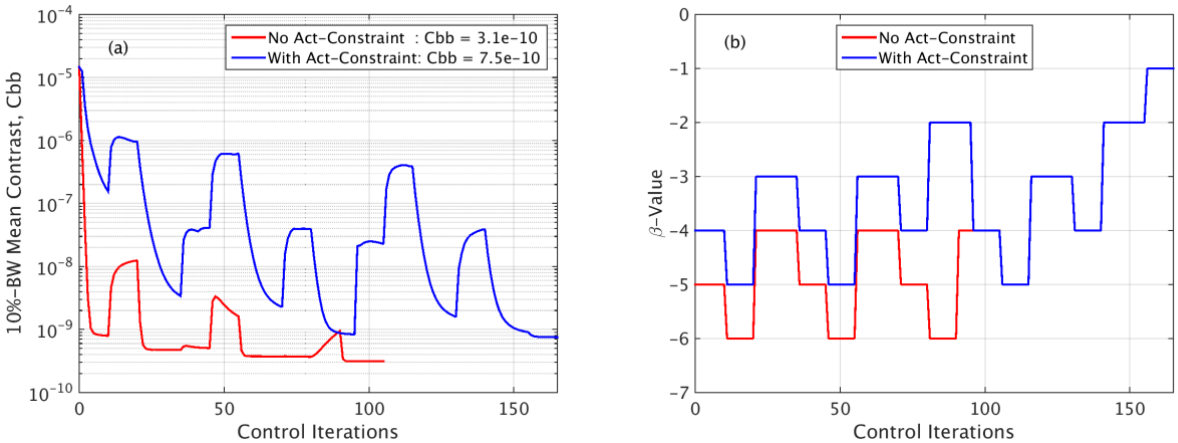

Figure 2. (a) Simulated C_{bb} –values versus control iteration number obtained without (red) and with (blue) actuator constraint. (b) The corresponding β-values used to obtain the results in part (a).

There are three sets of important parameters associated with each EFC simulation session: (1) Error state of the optical model, such as pupil amplitude and phase, and location and rotation parameters of DM1, DM2, occulting-mask and Lyot-Stop. (2) Initial actuator sensitivity matrices or Jacobians used. (3) Initial DM solutions used. We started the simulations presented in Figs. 2(a,b) with the following parameters: (1) Baseline state of the HLC [12], (2) a pair of final Jacobians obtained for the baseline model, and (3) the final DM solutions obtained for the error state referred to as "MC Error Case #1" in Table 1 of Ref. [12]. The initial $C_{bb} > 10^{-5}$ in Fig. 2(a) is a result of this mismatch between the model

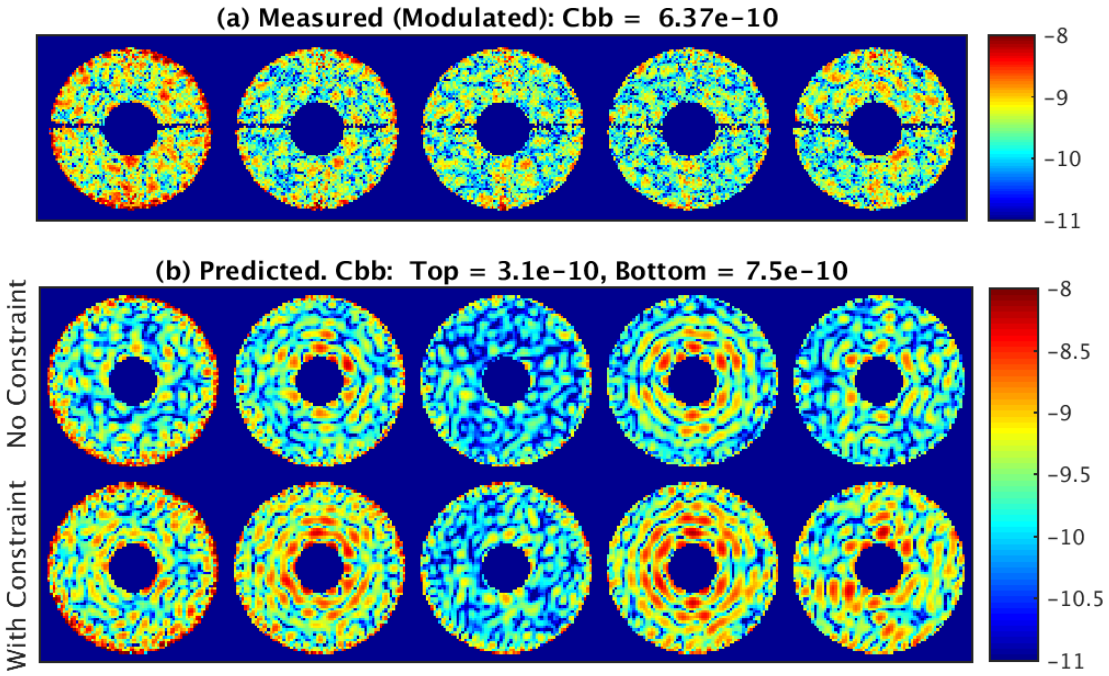

Figure 3. (a) Examples of the normalized intensities, $I(x,y)$, inside the $3 - 9\lambda_c/D$ dark-hole region measured on the HLC testbed. The 5 intensity maps correspond to five 2% narrowband beams centered at 528, 539, 550, 561 and 572nm, respectively. (b) Same as part (a), except that these maps are predicted monochromatic beam intensities corresponding to the last data points in Fig. 2(a).

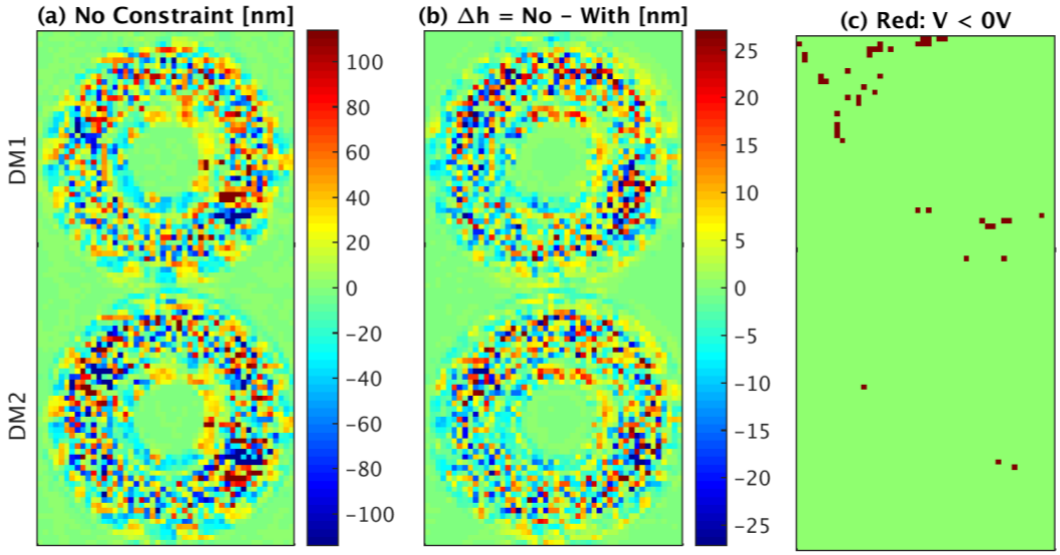

Figure 4. (a) The dark-hole components of the actuator heights corresponding to the red-curve last data point in Fig. 2(a). (b) Difference of the actuator heights corresponding to the last data points of the two curves in Fig. 2(a): No Constraint – With Constraint. (c) Location of the actuators of the "No Act-Constraint" case whose command values are outside the 0 – 100V range. There is no any actuator with V > 100V in this case, so only the actuators having V < 10V are shown with the red-markers in this plot.

and the actuator commands. There are many initial DM command options for us to choose from, and there is no any spatial reason for choosing the above one—We chose this particular one because it is convenient. It is a standard

procedure for our testbed team to update the DM1 and DM2 Jacobians after each EFC iteration. But in each case of Fig. 2(a), we updated the Jacobians only twice. For the case of not including actuator constraint, we updated the Jacobians after Iter = 35 and Iter = 70 ("Iter" means Iteration). Whereas for the case of including actuator constraint, we did so after Iter = 35 and Iter = 95.

Figure 3(a) shows an example of the normalized intensities measured on the HLC testbed. There are some explanations about the normalized intensity in Ref. [12]. Figure 3(b) shows the predicted results corresponding to the last data points in Fig. 2(a). The C_{bb}-values of these results listed in the figure titles are well within the testbed-model mismatch uncertainties.

Figure 4(a) shows the dark-hole components of the actuator heights corresponding to the last data point of the red-curve in Fig. 2(a), that is, the final DM actuator commands of the case not including the actuator constraint. Figure 4(b) shows the difference of the actuator heights corresponding to the last data points of the two curves in Fig. 2(a): No Constraint – With Constraint, and Fig. 4(c) shows the location of the actuators of the "No Act-Constraint" case whose command values are outside the 0 – 100V range. There is no any actuator with V > 100V in this case, so only the actuators having V < 10V are shown with the red-markers in this plot.

3. ACTUATOR GAIN CALIBRATION ERRORS

In this section we investigate the effects of actuator gain errors on the efficiency of EFC and the Zernike-mode error sensitivity of the HLC. In general, one can expect that the actuator height (h) versus actuator voltage (V) curve of each actuator is nonlinear and these curves are different for different actuators, as is evident from Figs. 1(c,d). Some preliminary measurements of the actuator response curves for an older version of the DM have indeed exhibited the evidence of such behavior, as is shown in Figs. 9(a-b) of Ref. [13]. Based on the knowledge learned from those measurements, a model of actuator nonlinear response curves with some random slope errors was proposed. It is expressed as

$$h_i(V_i, \delta_i) = (1+\delta_i)h(V_i), \qquad -50 \le h_i \le 50\text{V} \tag{1}$$

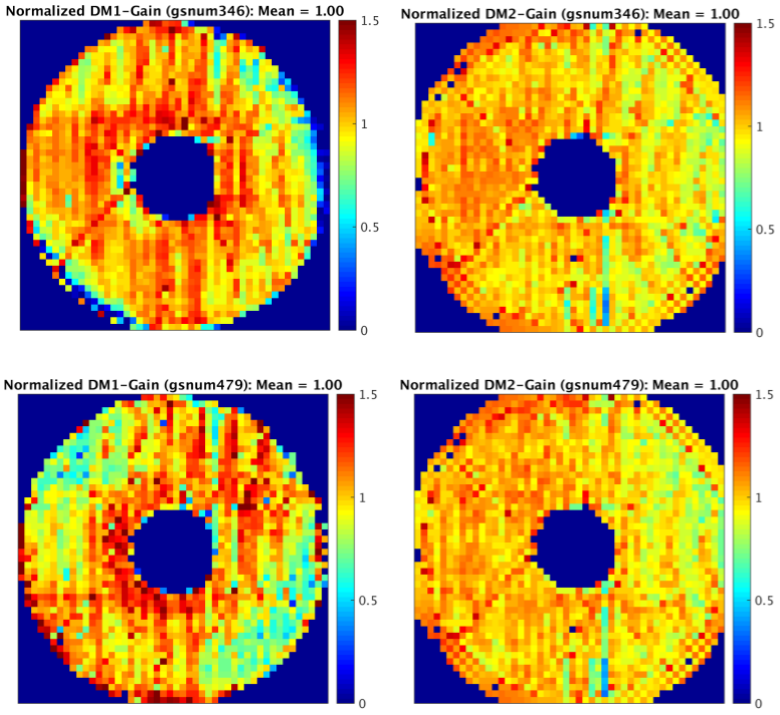

Figure 5. Two pairs of DM actuator gain maps measured on the OMC testbed. Only the date of the actuators used in the HLC model are shown. Each map is normalized by the mean value of the active actuator gains. The gain maps on the top-row (gsnum346) and the bottom-row (gsnum479) were measured in June and September of 2016, respectively.

where $h(V_i)$ is a 5th-order polynomial function of V_i that exhibits an "S-shape", and index i indicates the actuator number. In Ref. [13], δ_i were treated as normally-distributed random numbers obtained from the Matlab function *randn.m* and re-scaled the negative and positive parts separately such that $-0.3 \le \delta_i \le +0.3$. It was claimed in Ref. [13] that this range of the δ_i values roughly corresponds to the dh/dV data in Fig. 9(b) of Ref. [13] at V = 30V (for the 0 – 100V voltage range). That is, it was shown that the older version of the DM exhibited up to ±30% actuator gain non-uniformity.

The DM actuator gain maps similar to those shown in Figs. 1(c,d) were measured on the OMC testbed at JPL more than five times in the 2015 – 2017 time-period. Figure 5 shows two examples of the actuator gain maps measured more than two months apart from each other. If we calculate the difference of the DM1 and the DM2 gain maps in Fig. 5, and plot them as a histogram, we get Fig. 6. Although not shown here, the analysis of more than five sets of the measured actuator gain maps gave a total (DM1 plus DM2) gain variations or gain errors of $\sigma \sim 0.2$ (Standard Deviation, STD), similar to what we got in Fig. 6. It should be pointed out that when using a normal distribution for the actuator gain errors, the gain parameter δ and the gain error STD, σ, becomes approximately equal to each other.

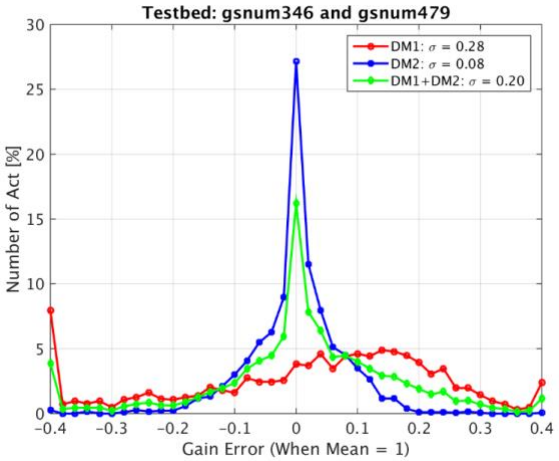

Figure 6. Histogram of the actuator gain changes obtained from the two pairs of the actuator gain maps in Fig. 5.

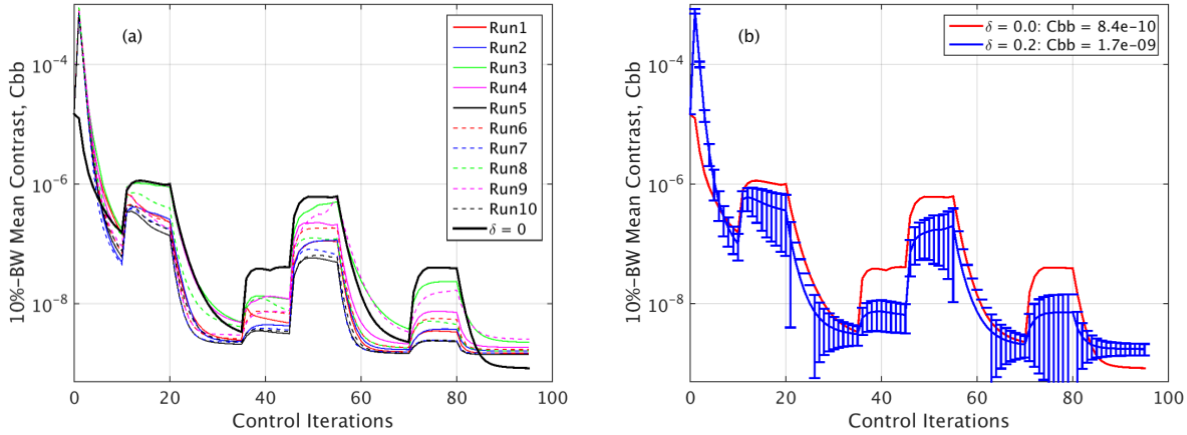

Figure 7. (a) Ten cases of C_{bb}–values versus control iteration number results obtained with random (normal-distribution) actuator gain errors having $\delta = 0.2$. The case of $\sigma = 0$ (thick black-curve) is the same as in Fig. 2(a) (up to Iter = 95 only) and is included here as a reference. (b) The mean values and the error-bars of the 10 random gain error runs shown in part (a) plus the C_{bb} -curve of the nominal case ($\delta = 0$). The error bars correspond to $\pm\sigma$.

In the following, we evaluate the impact of such gain errors on the efficiency of EFC as well as on the Zernike-mode error sensitivities of the HLC contrast.

3.1 Effects of the Actuator Gain Errors on EFC

We evaluated the effect of the actuator gain errors by repeating the EFC simulation of the blue-curve in Fig. 2(a) up to Iter = 95 for 10 different gain error realizations with $\delta = 0.2$, that is, by repeating the EFC simulations by including the actuator constraint and the normally-distributed actuator gain errors having a STD value of $\sigma = 0.2$. The results of those 10 individual cases as well as the nominal case ($\delta = 0$) are shown in Fig. 7(a), and the mean values and the error bars ($\pm\sigma$) of the 10 gain error runs are shown in Fig. 7(b). In these simulations, we converted the actuator heights into voltage based on the gain maps in Fig. 1(c,d) when applying the actuator constraint, but applied the actuator gain errors directly to the actuator heights before calculating the dark-hole e-field for the next EFC iteration, assuming linear response curves for all actuators. As we can see from Fig. 7(b), the $\delta = 0.2$ gain errors degrade the contrast floor by about 2x.

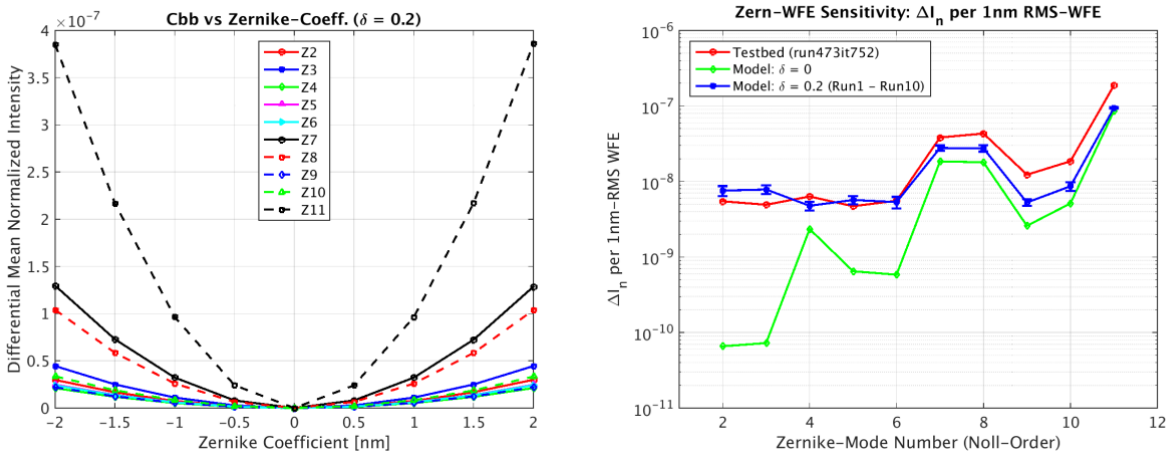

Figure 8. (a) Mean normalized intensity, I_n, versus Zernike-coefficient when the actuator gain errors with $\delta = 0.2$ is included. This is just one realization and is shown here as an example. The nominal value of I_n at Zi = 0nm corresponds to the last data point of the blue-curve in Fig. 2(a). (b) One set of HLC testbed results of a_2 versus Zernike-mode number and the corresponding model predictions. The simulated results include the nominal case ($\delta = 0$) as well as the mean and the error bars of ten actuator gain error realizations with $\delta = 0.2$. The error bars correspond to $\pm\sigma$.

3.2 Effects of the Actuator Gain Errors on Low-Order WFE Sensitivities of the HLC

It is expected that the low-order WFE of the WFIRST coronagraph will drift over time during its operation. In order to understand the impact of such drift on the coronagraph contrast performance, our OMC testbed team at JPL measured the Zernike-mode sensitivities of the OMC broadband contrast. In doing so they followed these steps:

(1) Obtain a contrast floor of $C_{bb} \sim 10^{-9}$ (modulated component)

(2) Dial-in Zernike-modes $Z_2 - Z_{11}$ by commanding the DM2 actuators accordingly, one mode at a time, and vary the Zernike-coefficient value, Z_i, in the [-2 2] nm range with an increment of 0.5nm. Record the open-loop values of the measured mean normalized intensity, I_n

(3) Fit second-order polynomial to I_n vs Z_i in the form of

$$I_n(Z_i) = a_2 Z_i^2 + a_1 Z_i + a_0 \qquad (2)$$

(4) Plot a_2 as a function of Zernike-mode number (Noll-order).

Figure 8(a) shows a set of examples of the predicted mean normalized intensity, I_n, versus Zernike-coefficient. They were obtained by including actuator gain errors with $\delta = 0.2$. The red-curve in Fig. 8(b) shows one set of a_2 versus Zernike-mode number data measured on the HLC testbed. If we do not include the actuator gain errors, we obtain the model prediction shown with the green-curve in Fig. 8(b). In that case the predicted a_2 is off a lot from the testbed data for Zernike-modes of $Z_2 - Z_6$. However, the agreement between the measured and the predicted results improve a lot if we include the actuator gain errors with $\delta = 0.2$, as shown with the blue-curve in Fig. 8(b). It is the mean of 10 different gain error realizations and the error bars correspond $\pm\sigma$.

4. CONTRAST FLOOR AND CHROMATICITY: MODEL VERSUS TESTBED

One of the OMC project goals is to validate the model against the testbed results. In order to come up with realistic model predictions on broadband contrast floor and narrowband contrast chromaticity, we carried out 10 runs of Monte-Carlo (MC) EFC simulations starting from the baseline conditions. The names and the values of the parameters used in those 10 runs are listed in Table 1. The parameters of the first run, "MC-#1", are identical to those listed as "Monte-Carlo Error Case #1" in Table 1 of Ref. [12]. The pupil amplitudes numbered 1 – 10 were measured on the OMC testbed at different times relative to the baseline case. At the beginning, we calculated the difference of the baseline pupil phase map and another one measured at a different time, and from that differential phase map we obtained 60 Zernike-mode coefficients and a set of Power-Spectral Density (PSD) error parameters. After that we obtained 10 sets of differential phase maps by varying those Zernike coefficients and the PSD parameters randomly. Finally we added those differential phase maps to the baseline one to generate phase maps for 10 MC runs. In Table 1 of Ref. [12], the "MC Error RMS" column shows the RMS values of the Monte-Carlo errors used to generate the corresponding 10 sets of the random

Table 1. Names and values of 10 random error sets used in our MC simulations. "MC" means Monte-Carlo, and "Meas" means "Measured".

	DM1			DM2			Occ		Lyot		Amplitude	Phase
MC-#	Tx	Ty	Rz	Tx	Ty	Rz	Tx	Ty	Tx	Ty		
1	-26	-35.9	-0.06	-42.8	-45.9	0	-0.3	0.4	34.2	3.4	Meas-1	Meas0 + Synthesized-1
2	20.1	58.5	-0.02	19.5	10.7	-0.04	-0.2	-0.3	-18.6	-29.5	Meas-2	Meas0 + Synthesized-2
3	-4.2	-47.3	-0.01	-26.7	62.7	-0.04	0.7	-0.1	-5.1	13.6	Meas-3	Meas0 + Synthesized-3
4	-65.6	47.1	-0.02	50.3	-15.6	0	-0.3	0	-17.3	-19.7	Meas-4	Meas0 + Synthesized-4
5	-57.5	-12.1	-0.06	6.4	21.6	0.06	0.7	-0.3	2.1	8.6	Meas-5	Meas0 + Synthesized-5
6	-37.5	16.1	0.04	62.4	-2.1	0.02	0.1	-0.7	20.2	3.3	Meas-6	Meas0 + Synthesized-6
7	39.4	68.4	-0.04	-5.9	-13.1	-0.01	0.3	-0.3	14	19.2	Meas-7	Meas0 + Synthesized-7
8	-2.8	58.6	-0.03	-54.5	-4.8	-0.01	0.3	-0.6	12.1	-32.8	Meas-8	Meas0 + Synthesized-8
9	-3.4	36.2	0	4.7	58.7	-0.01	0.1	0.7	-21.4	24.1	Meas-9	Meas0 + Synthesized-9
10	48	-62.5	-0.06	55.2	67.7	0.02	0.7	0	-3	4.2	Meas-10	Meas0 + Synthesized-10
Unit	um	um	deg	um	um	deg	um	um	um	um		

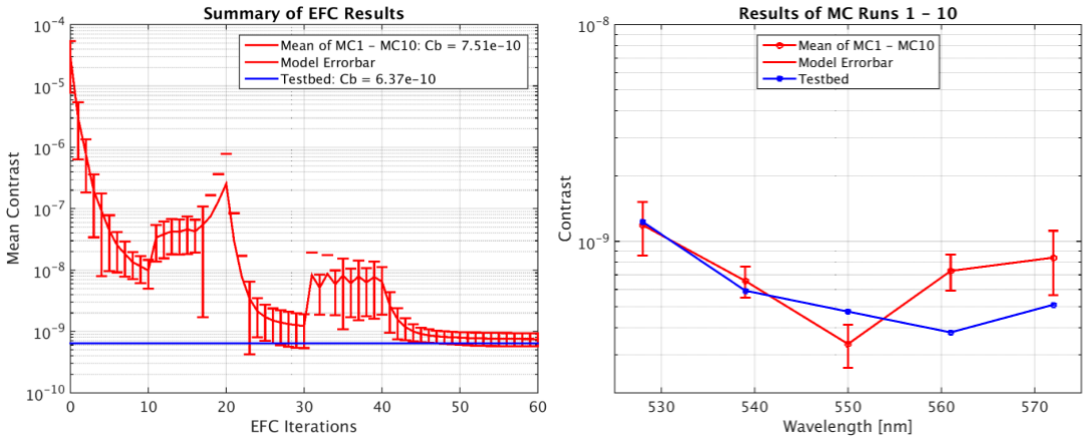

Figure 9. (Left) Mean of the ten MC cases of C_{bb}–value versus control iteration number results predicted by our HLC model. The actuator gain errors are not included in these simulations. The error bars show ±σ. The blue-line represents the HLC testbed result reported in Milestone 9 review. (Right) The corresponding narrowband contrast chromaticity. Again, the error bars correspond to ±σ.

Figure 9(left) shows the mean values and the error bars of the C_{bb} versus control iteration number data obtained from the 10 MC runs, and Fig. 9(right) shows the corresponding narrowband chromaticity. The testbed results reported in

Milestone 9 review are also shown for the purpose of comparison. On the HLC testbed, the chromaticity data were measured by using five 2%-BW filters centered at 528, 531, 550, 561 and 572nm, whereas the model predictions were obtained with the corresponding monochromatic beams. Figure 10(left) shows the ratio of the chromaticity data, testbed divided by the model. As we can see, the ratio is within a factor of 2 at all 5 wavelength bands.

The OMC testbed team uses a pair-wise, deformable mirror, image plane-based diversity method to estimate the image-plane complex e-fields from measured intensities. But we have access to the complex e-field directly in our model. In order to reduce the computation time, we did not carry out e-field estimation when obtaining the results presented in this paper. On the other hand, as we can see from the results in Fig. 10(right), no-probing or no e-field estimation produces results that are very close to the case of probing. In this figure, we plotted the final C_{bb} results of the 10 MC runs obtained with and without probing.

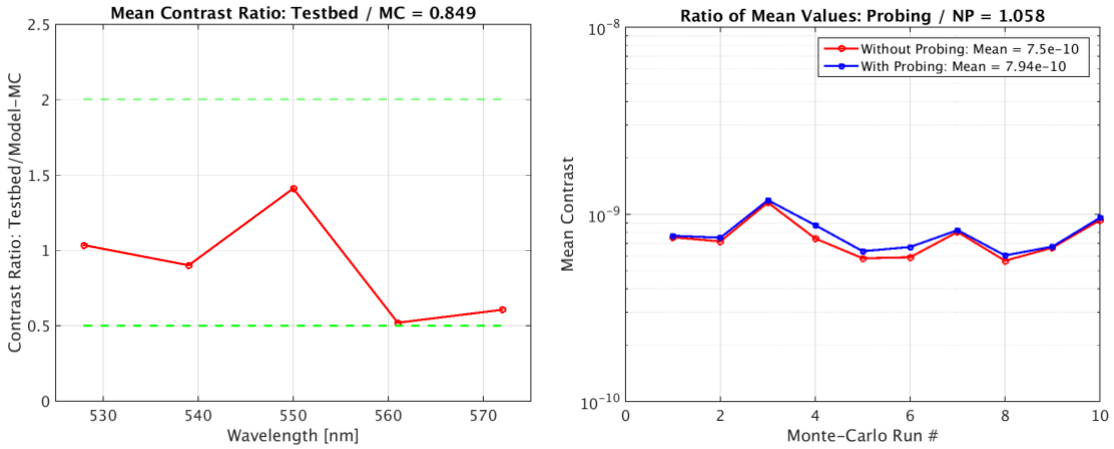

Figure 10. (Left) The ratios of the narrowband contrast chromaticity: Testbed/Model. (Right) Comparison of final C_{bb} – values of the 10 Monte-Carlo EFC simulation runs obtained without and with e-field estimation.

5. CONCLUSION

The Occulting Mask Coronagraph testbed at JPL operates in two different modes: A Hybrid Lyot Coronagraph (HLC) and a Shaped-Pupil Coronagraph (SPC). The HLC testbed has completed Milestone 9 with a mean, 10%-broadband total (modulated plus unmodulated) contrast value of $1.6\text{x}10^{-9}$ at a center wavelength of 550nm in a 360-deg dark-hole region covering $3 - 9\lambda_c/D$ field angle. One of the OMC project goals is to validate the model against the testbed results. In order to come up with realistic model predictions on broadband contrast floor and narrowband contrast chromaticity, we introduced two actuator constraints, one on the command range and the other on the neighboring actuator rule, and also interconnected two pairs of actuators on DM1 as was detected on the OMC testbed. When we carried out EFC simulations with the above actuator constraints and the DM1 actuator defects using the measured pupil amplitude and phase and also matching the other model parameters as best as we can with the testbed, we obtained a 10% bandwidth broadband mean contrast of $C_{bb} = 7.5\text{x}10^{-10}$. One of the best results obtained on the HLC static testbed is $C_{bb} = 6.4\text{x}10^{-10}$ (modulated component), and the above model prediction agrees well with this measurement result.

More than 5 sets of DM1 and DM2 actuator gain maps measured on the OMC testbed during a time span of ~2 years showed changes (including the measurement errors) on the order of $\delta \sim 0.2$ (standard deviation). We carried out 10 runs of Monte-Carlo EFC simulations with such actuator gain errors, and showed that the C_{bb}–value degrades by about 2x as compared to the nominal ($\delta = 0$) case.

One of the measurements carried out on the OMC is the Zernike-mode error dependence of the 10%-BW broadband mean contrast, or the sensitivity of the broadband contrast on $Z_2 - Z_{11}$ Zernike-mode errors. When we did not include the DM actuator gain errors in simulations, the predicted $Z_2 - Z_6$ sensitivities of the HLC contrast did not agree well with the testbed results. But when we included $\delta = 0.2$ actuator gain errors in the simulations, the agreement between the predicted and the measured results was greatly improved and reached to an acceptable level.

We also carried out 10 runs of Monte-Carlo EFC simulations by randomly changing DM1 and DM2 position and clocking parameters as well as Occulting-Mask and Lyot-Stop position parameters. The average value of the broadband mean contrast, C_{bb} = $7.51x10^{-10}$, again agreed well with the testbed result, and the predicted narrowband contrast chromaticity also agreed with the measured results within a factor of two.

We believe the results of this study validate our HLC model reasonably well.

The research was carried out at the Jet Propulsion Laboratory, California Institute of Technology, under a contract with the National Aeronautics and Space Administration.

REFERENCES

[1] *John Trauger, Dwight Moody, Brian Gordon*, "Complex apodized Lyot coronagraph for exoplanet imaging with partially obscured telescope apertures," Proc. SPIE 8864, 886412 (2013).
[2] John Krist, "End-to-end numerical modeling of AFTA coronagraphs," Proc. SPIE 9143, 91430V (2014).
[3] Byoung-Joon Seo, *et al*, "Hybrid Lyot coronagraph for wide-field infrared survey telescope-astrophysics focused telescope assets: Occulter fabrication and high contrast narrowband testbed demonstration," metrics," J. Astron. Telesc. Instrum. Syst. 2(1), 011019 (2015).
[4] John Trauger, Dwight Moody, John Krist, and Brian Gordon, "Hybrid Lyot coronagraph for WFIRST-AFTA: coronagraph design and performance metrics," J. Astron. Telesc. Instrum. Syst. 2(1):011013 (2016).
[5] A. Carlotti, N.J. Kasdin, and R. Vanderbei, "Shaped pupil coronagraphy with WFIRST-AFTA," Proc. SPIE 8864, 886410 (2013).
[6] Eric Cady, *et al*, "Demonstration of high contrast with an obscured aperture with the WFIRST-AFTA shaped pupil coronagraph," J. Astron. Telesc. Instrum. Syst. 2(1):011004 (2015).
[7] Olivier Guyon, "Imaging Earth-like planets around late-type stars with low-inner working angle PIAA coronagraphy," Proc. SPIE 8864, 886414 (2013).
[8] Brian Kern, *et al*, "Phase-induced amplitude apodization complex mask coronagraph mask fabrication, characterization, and modeling for WFIRST-AFTA," J. Astron. Telesc. Instrum. Syst. 2(1):011014 (2016).
[9] Amir Give'on *et al*, "Broadband wavefront correction algorithm for high-contrast imaging system," Proc. SPIE, **6691**, 66910A (2007).
[10] A. Give'on, B. D. Kern, and S. Shaklan, "Pair-wise, deformable mirror, image plane-based diversity electric field estimation for high contrast coronagraphy," Proc. SPIE 8151, 815110 (2011).
[11] John Krist, Bijan Nemati, and Bertrand Mennesson, "Numerical modeling of the proposed WFIRST-AFTA coronagraphs and their predicted performances," J. Astron. Telesc. Instrum. Syst. 2(1):011003 (2016).
[12] Erkin Sidick, Byoung-Joon Seo, Brian Kern, David Marx, Ilya Poberezhskiy, and Bijan Nemati, "Sensitivity of WFIRST coronagraph broadband contrast performance to DM actuator errors," Proc. SPIE, SPIE Conference 10400-6, August 2017
[13] E. Sidick, S. Shaklan, A. Give'on, and B. Kern, " Studies of the effects of actuator errors on the HCIT/PIAA contrast performance ," Proc. SPIE, vol. 7731, pp.7731-4T, June 2010.
[14] E. Sidick, S. Shaklan, and Eric Cady, " High-contrast coronagraph performance in the presence of DM actuator defects ," Proc. SPIE, vol. 9605, pp.96051Y, August 2015.
[15] Erkin Sidick, and F. Shi, "Effect of DM actuator gain errors on the WFIRST/AFTA coronagraph contrast performance," Proc. SPIE, vol. 9605, pp. 960506, August 2015.
[16] Erkin Sidick, Byoung-Joon Seo, David Marx, Ilya Poberezhskiy, and Bijan Nemati, "WFIRST/AFTA Coronagraph Contrast Performance Sensitivity Studies: Simulation versus Experiment," Proc. SPIE, vol. 9912, pp. 99126M, August 2016.